AGU PUBLICATIONS

Geophysical Research Letters

RESEARCH LETTER
10.1002/2013GL058681

Key Points:
- First time airborne radio occultation shown to agree with independent data
- First time airborne RO measurements have been collected in a tropical storm
- It demonstrates the potential for an operational system on commercial aircraft

Supporting Information:
- Text S1

Correspondence to:
J. S. Haase,
jhaase@ucsd.edu

Citation:
Haase, J. S., B. J. Murphy, P. Muradyan, F. G. Nievinski, K. M. Larson, J. L. Garrison, and K.-N. Wang (2014), First results from an airborne GPS radio occultation system for atmospheric profiling, *Geophys. Res. Lett.*, *40*, doi:10.1002/2013GL058681.

Received 11 NOV 2013
Accepted 3 FEB 2014
Accepted article online 6 FEB 2014

First results from an airborne GPS radio occultation system for atmospheric profiling

J. S. Haase[1], B. J. Murphy[2], P. Muradyan[2], F. G. Nievinski[3], K. M. Larson[4], J. L. Garrison[5], and K.-N. Wang[5]

[1]Scripps Institution of Oceanography, University of California, San Diego, La Jolla, California, USA, [2]Department of Earth, Atmospheric, and Planetary Sciences, Purdue University, West Lafayette, Indiana, USA, [3]Faculdade de Ciências e Tecnologia, Universidade Estadual Paulista, Presidente Prudente, Brazil, [4]Department of Aerospace Engineering Sciences, University of Colorado Boulder, Boulder, Colorado, USA, [5]Department of Aeronautics and Astronautics Engineering, Purdue University, West Lafayette, Indiana, USA

Abstract Global Positioning System (GPS) radio occultation (RO) from low Earth-orbiting satellites has increased the quantity of high-vertical resolution atmospheric profiles, especially over oceans, and has significantly improved global weather forecasting. A new system, the Global Navigation Satellite Systems Instrument System for Multistatic and Occultation Sensing (GISMOS), has been developed for RO sounding from aircraft. GISMOS also provides high-vertical resolution profiles that are insensitive to clouds and precipitation, and in addition, provides greater control on the sampling location, useful for targeted regional studies. The feasibility of the system is demonstrated with a flight carried out during development of an Atlantic tropical storm. The data have been evaluated through a comparison with dropsonde data. The new airborne RO system will effectively increase by more than 50% the number of profiles available for studying the evolution of tropical storms during this campaign and could potentially be deployed on commercial aircraft in the future.

1. Introduction

GPS radio occultation uses radio signals to sense the atmosphere as a transmitting GPS satellite sets behind or rises above the horizon relative to a moving receiver (Figure 1). The radio waves undergo refractive bending and a Doppler shift due to variations of refractive index within the atmosphere primarily in the vertical direction. The refractive index in the neutral atmosphere depends on the pressure (hPa), P, temperature (K), T, and water vapor partial pressure (hPa), e,

$$N = (n-1) \times 10^6 = \frac{77.6890P}{T} - \frac{6.3938e}{T} + \frac{3.75463 \times 10^5 e}{T^2} \quad (1)$$

[*Rüeger*, 2002]. Thus, information on the structure of the atmosphere can be retrieved from precise measurements of the amplitude and Doppler shift of the radio waves.

GPS/MET was the first mission to demonstrate that profiles could be retrieved for the Earth's atmosphere using this technique [*Kursinski et al.*, 1996]. Since then, several missions have been launched, most notably the Constellation Observing System for Meteorology Ionosphere and Climate (COSMIC)/Formosa Satellite-3 (FORMOSAT-3) constellation [*Anthes et al.*, 2008], which provides radio occultation (RO) observations on a routine basis. Operationally, spaceborne RO data have improved global numerical weather model forecasts [*Healy and Thepaut*, 2006; *Poli et al.*, 2008]. However, RO data have only brought limited improvement on regional short-term weather simulations and forecasts of high-impact weather in tropical storms [*Kueh et al.*, 2009]. One reason for this is that for targeted areas, spaceborne RO sampling in time and space is still relatively sparse. For example, in a case study of the 2006 Typhoon Kaemi [*Chen et al.*, 2009], only seven RO profiles were available within the 6000 km × 6000 km model domain and within ± 3 h of the initialization time. The closest profile was more than 600 km from the typhoon center, and the overall impact on the forecast track and rainfall was inconclusive. Other studies have investigated the impact of spaceborne RO in forecasting tropical cyclones [*Huang et al.*, 2005; *Kueh et al.*, 2009] and have shown that localized regions where the moisture increment is high relative to the first guess model have produced significant changes in low-level and midlevel circulations. In a study showing positive results for the 2006 Hurricane Ernesto, assimilation of GPS RO profiles during the 2 days before hurricane genesis resulted in an improvement of the hurricane intensification forecast [*Liu et al.*, 2012].

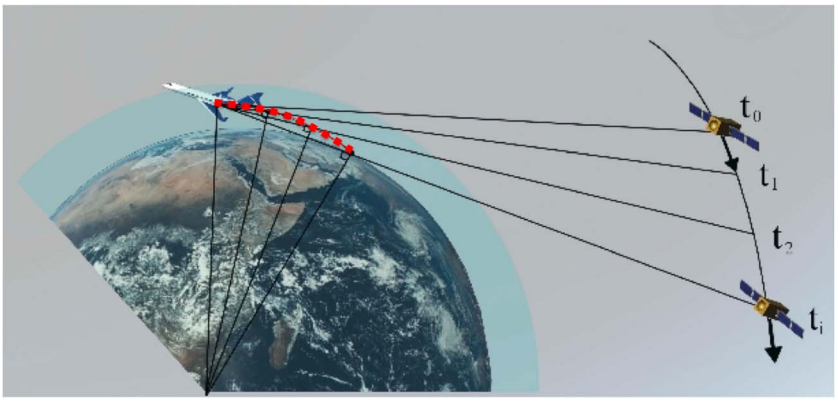

Figure 1. Airborne radio occultation geometry. GPS signals are recorded as a GPS satellite sets, with raypaths successively sampling deeper into the atmosphere or successively shallower as a GPS satellite rises. The tangent points are the points of closest approach of each raypath to the Earth's surface. The consecutive points are indicated by red dots, which drift horizontally away from the aircraft as altitude decreases for a setting satellite. The atmosphere is most dense at the tangent point, so the measured refractive delays are most strongly influenced by the atmospheric properties at this location. Retrievals of atmospheric refractivity are represented as values along these slanted tangent point profiles.

As in several other cases, the improvement was shown to be a result of assimilating only a few key RO profiles, by chance located nearby and upstream of the storm [*Huang et al.*, 2010; *Liu et al.*, 2012].

While the results of some of these individual cases are promising, the number of cases where an RO profile is serendipitously located near a developing system is very limited. One of the primary motivations for developing an airborne RO system is that the locations of the occultation profiles will occur near the flight track (within 250 km), so that the potential impact of denser sampling of RO profiles near the center of a storm system can be tested. In addition, spaceborne RO observations in the lower troposphere are typically down weighted during assimilation relative to upper troposphere and lower stratosphere observations because of the potentially larger errors attributed to assuming local spherical symmetry in the retrieval process. The airborne system has the potential to provide the data necessary to investigate these errors in detail while simultaneously providing a platform for easily collecting independent collocated measurements.

For a receiver within the atmosphere, the RO technique differs from the spaceborne technique [*Zuffada et al.*, 1999] in that the raypath through the neutral atmosphere is not symmetric with respect to the tangent point (point of closest approach to the Earth). The retrieval technique has been adapted to the airborne geometry and several simulation studies have been carried out [*Healy et al.*, 2002; *Lesne et al.*, 2002; *Xie et al.*, 2008]. An exploratory flight system was tested in Japan [*Yoshihara et al.*, 2006]; however, only qualitative conclusions about the performance were drawn. Here we report the first results to provide a quantitative evaluation of the airborne GPS RO measurement technique and illustrate its first use in tropical storms.

2. Measurement Campaign

The Global Navigation Satellite Systems (GNSS) Instrument System for Multistatic and Occultation Sensing (GISMOS) was deployed in August–September 2010 for the Pre-Depression Investigation of Cloud systems in the Tropics (PREDICT) [*Montgomery et al.*, 2012]. The objective of the campaign was to investigate the thermodynamics and circulation within the interior of African easterly waves prior to development of tropical storms. While not all African easterly waves develop into hurricanes, more than 80% of major hurricanes originate as easterly waves [*Landsea*, 1993]. Few in situ observations have been made of tropical systems within easterly waves during the transition from disorganized convection to tropical depression because development usually happens far from shore, over the Atlantic. This experiment targeted early measurements in the wave axis where the mean flow and wave speed were similar, leading to the isolation of areas where atmospheric moisture potentially could be concentrated [*Dunkerton et al.*, 2008; *Wang et al.*, 2010]. The National Science Foundation (NSF) Gulfstream-V aircraft flew six research flights into the tropical disturbance that eventually developed into Hurricane Karl. On 8 September, as an easterly wave approached the windward islands, it merged with a trough over South America to produce a broad area of low pressure, which then

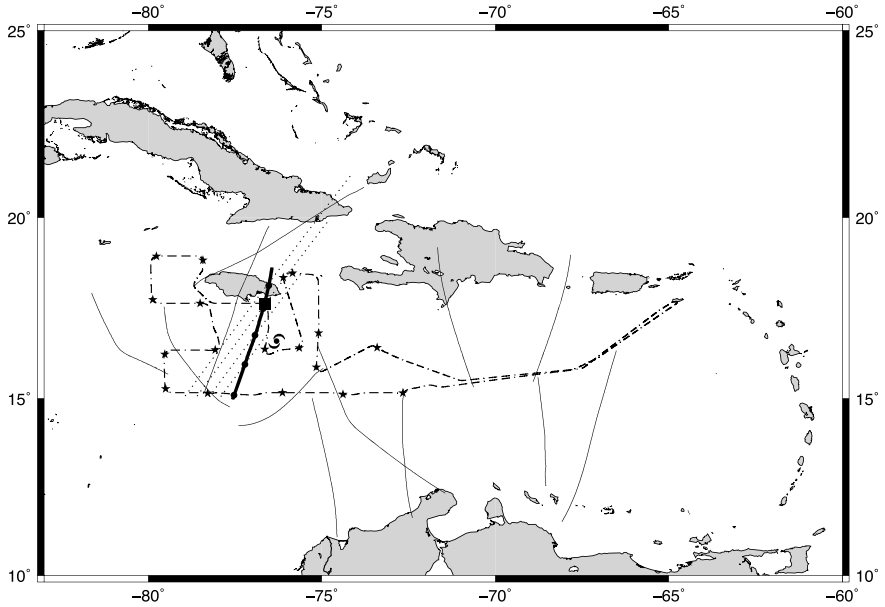

Figure 2. Aircraft flight path for RF18 over the Caribbean Sea on 13 September 2010 (dash-dotted line), location of dropsonde released on 13 September 2010 at 13:24 UTC (large square), and other dropsondes (stars). For each occultation, the horizontal locations of the tangent points are shown (thin black lines), starting from the highest tangent point adjacent to the flight path and ending at the lowest tangent point furthest from the aircraft. The occultation of PRN25, is shown as a bold black line; for this event, the line of sight from the aircraft to the setting GPS satellite at consecutive times is shown with dotted lines (defined in the text). The hurricane symbol indicates the center of the tropical disturbance at 12:00 UTC before it developed into Hurricane Karl.

moved westward producing disorganized convection. Late on 13 September the central convection increased and a closed circulation developed, forming a tropical depression around 12:00 UTC on 14 September [*Stewart*, 2011], several days later than anticipated. We have analyzed data from research flight RF18 from 10:00 to 16:00 UTC on 13 September 2010, the fifth of six research flights into the storm system. In situ pressure and temperature measurements were made at flight level, and dropsondes were released during this research flight in order to sample the thermodynamic profiles and the winds in the interior of the wave as the circulation developed. During the flight, the GISMOS system made continuous observations of GPS signal carrier phase at 5 Hz using conventional geodetic receivers and recorded the GPS raw RF signal at 10 MHz from side-looking antennas [*Garrison et al*., 2007]. An Applanix POS/AV^{TM} inertial navigation system was used to achieve velocity precision better than 5 mm/s as required for accurate airborne retrievals [*Muradyan*, 2012; *Muradyan et al*., 2010; *Xie et al*., 2008]. GISMOS measurements of the excess GPS signal propagation delay were used to derive profiles of atmospheric refractivity, which is directly related to moisture and temperature (see the supporting information for full details of the method).

3. Results

The aircraft flew at an average altitude of ~ 14 km in a lawn mower pattern over the central region of deep convection (Figure 2). During this time, satellite PRN25 set beyond the horizon at ~11:40 UTC, producing an occultation on the starboard side of the aircraft. The line of sight from the aircraft to the setting GPS satellite at consecutive times is shown in Figure 2 (dotted lines), for the segment of the raypath passing through the atmosphere below the aircraft height. The tangent point is the closest point to the surface of the Earth along the raypath (Figures 1 and 2). The highest tangent point of the occultation is located at the aircraft position and drifts farther from the aircraft as the satellite sets, in this case drifting 327 km at the lowest point tracked. The bold line in the figure connects these tangent points at successively lower height. Since the accumulated refractive bending or delay is greatest where the atmosphere is the densest, the measurement is most sensitive to the refractivity at the tangent point, although it samples the entire path illustrated by the dotted lines. The retrieved refractivity profile is therefore not vertical but slanted along the direction of the

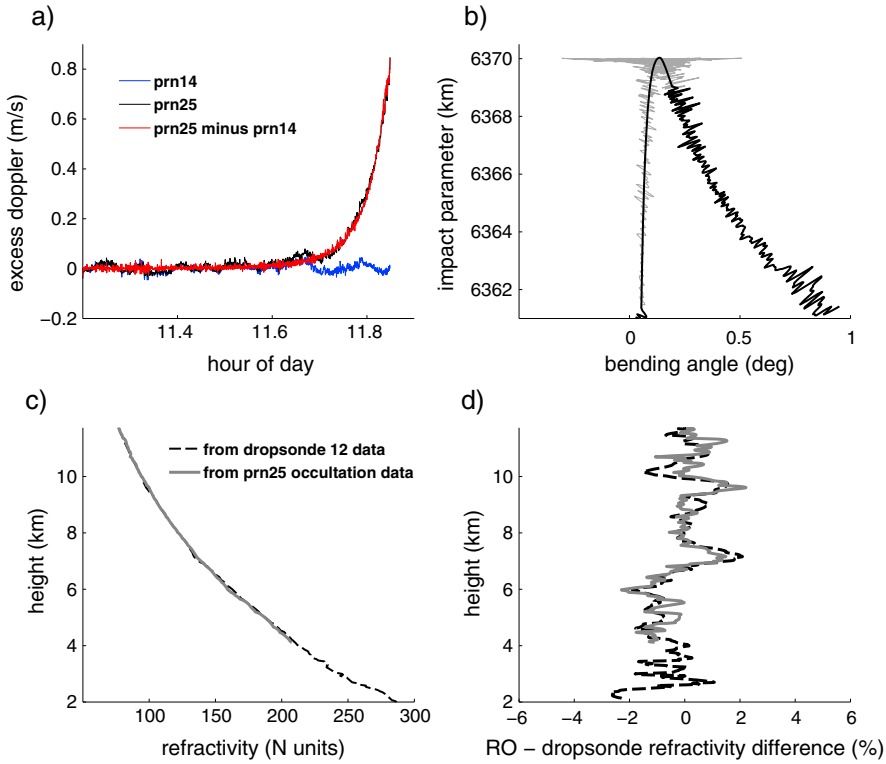

Figure 3. (a) Excess Doppler shift for the occulting satellite PRN25 (black) and a reference high-elevation angle satellite PRN14 (blue) for recordings made on 13 September 2010 during RF18. The difference in the excess Doppler (red), PRN25 minus PRN14, removes variations due to the receiver clock. (b) Bending angle (gray) derived from the excess Doppler shift. Noise due to turbulence creates large errors in bending angle near the maximum impact parameter. Bending angle values are replaced with simulated values for impact parameters above 1 km below the maximum impact height (black; see supporting information). (c) Retrieved RO refractivity (black) compared to the refractivity calculated from dropsonde 12 released on 13 September 2010 at 13:24 UTC (dashed). (d) RO minus dropsonde percent refractivity difference for the conventional geodetic receiver (gray) and the open loop method (black dashed line).

tangent point drift. This sampling geometry can be handled in a straightforward manner in data assimilation by assigning the observation to the horizontal location of the tangent point. The locations of the dropsondes released on this flight are also shown in Figure 2 (stars).

Our approach is to directly compare the retrieved refractivity with refractivity derived from the nearest dropsonde profile, in order to address the accuracy of the measurement with as few assumptions as possible. The Doppler shift of the setting satellite PRN25 is shown in Figure 3a, along with the Doppler of PRN14 used to correct for receiver clock errors. The final retrieved refractivity is derived using the method described in the supporting information, and is shown in Figure 3b. It is compared to the refractivity calculated from dropsonde 12 that was released during the same flight at 13:24 UTC at −76.640300°E, 17.642200°N. The dropsonde horizontal location was 25 km from the deepest tangent point of the occultation profile. GISMOS sampled tangent point altitudes in the height interval 14 km to 4 km for PRN25. The difference in refractivity between the dropsonde measurement and the occultation measurement is less than 2%. The agreement with the dropsonde is comparable to the accuracy of COSMIC spaceborne RO observations in the lower troposphere. *Chen et al.* [2011] estimated COSMIC measurement accuracy using the National Meteorological Center method [*Parrish and Derber*, 1992], which is based on comparing apparent errors with an estimate of the model errors from lagged forecast differences. The COSMIC refractivity errors were shown to vary approximately linearly from 0.5% at 10 km to about 2.5% at the surface, in summer months and at latitudes south of 45°.

We use the entire set of dropsondes released on the 13 September 2010 flight to examine a concern that is often raised with RO measurements: that the horizontal resolution is insufficient to be useful for mesoscale systems, especially tropical storms. While the horizontal resolution is certainly limited, several studies have

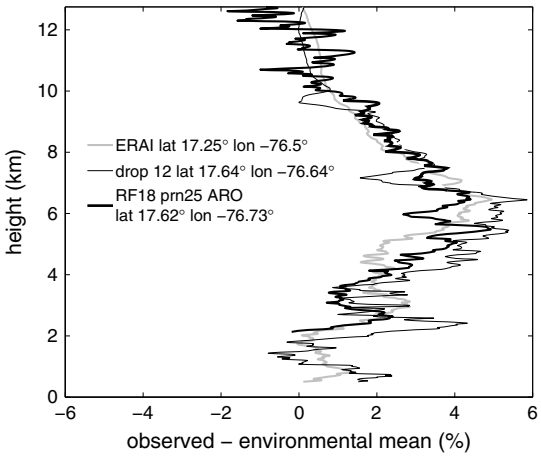

Figure 4. RO refractivity profile (bold black line) deviation relative to the environmental mean, defined as the mean refractivity profile for 11 dropsondes released 13 September 2010 (the zero reference). Despite the averaging inherent in the RO measurement, the refractivity local to the tangent point (bold) is significantly closer to the nearby dropsonde (thin black line) than to the environmental mean profile at 0%. The RO profile is also close to the ERA-Interim (ERAI) reanalysis profile at the closest grid point to the lowest tangent point.

indicated that spaceborne RO profiles assimilated into weather models near tropical cyclones have improved forecasts [*Huang et al*., 2010; *Liu et al*., 2012]. In this case we quantify the agreement of the RO profile with the nearest dropsonde (#12), and compare that with the agreement with the overall suite of dropsondes. The average background refractivity profile in the study area was calculated from 11 dropsondes within 520 km of the RO profile (Figure 2) and was used as the reference. Figure 4 shows that both dropsonde 12 and the RO profile have significantly higher refractivity than the background (at zero line), which we attribute to higher moisture in the altitude range from 4 to 8 km. Thus, we demonstrate that the difference between the RO profile and dropsonde 12, which we can consider an estimate of the accuracy, is better than the range of the horizontal refractivity variations that are important in the midtropospheric levels of this developing system. As an additional validation, we include in the comparison the European Center for Medium-Range Weather Forecasting Reanalysis-Interim (ERAI) at 0.75° resolution, which assimilated the dropsonde data that were transmitted via the Global Telecommunication System for operational use during the campaign. ERAI closely agrees with the RO profile and the dropsonde profile in this altitude range where moisture variations are important. The RO profile below 9 km agrees more closely with the ERAI profile than the dropsonde profile, even though the dropsonde was assimilated. We suggest that the dropsonde often shows a greater difference from the ERAI model because of representativeness errors, that is, the dropsonde point measurement is not representative of the atmosphere at the scale of the model grid. This has been described in assimilation tests that compare the impact of dense profile data averaged over 10 km compared to 40 km [*Frehlich*, 2011; *Weissmann and Cardinali*, 2007]. RO observations, on the other hand, naturally average over this spatial scale and thus might be expected to agree better with the ERAI analysis.

Finally, we have also compared the level of agreement between the dropsonde and RO profile with the expected range of variations empirically observed to be important for cyclone development. Specifically, *Komaromi* [2013] estimated the variation of the daily mean dropsonde profile relative to the background mean for developing versus nondeveloping cases from the PREDICT campaign and found that, on average, the nondeveloping cases had a significant dry humidity anomaly present between 300 hPa and 950 hPa, with a maximum mixing ratio anomaly of −1 g/kg at 550 hPa. This corresponds to a refractivity anomaly of −3% at 550 hPa, which is of the order that can be distinguished by the airborne RO method. In addition, within 150 km of the center of circulation for the genesis events, the moisture between 300 hPa to 950 hPa increased by ~ 1 g/kg, creating an expected change in refractivity on the order of 2–3.5%. While the RO profile has relatively poor horizontal resolution compared to dropsondes, it does give an average refractivity observation near the tangent point that captures the scale of spatial and temporal anomalies shown by *Komaromi* [2013] to be important and is thus expected to be useful for measuring the general thermodynamic properties in the interior of tropical storm systems, despite its inability to resolve smaller-scale convective features.

In the lowest part of the atmosphere, strong refractivity gradients can lead to complex signal propagation effects causing signal fading and rapid carrier phase fluctuations. The signal variations can exceed the operational range of conventional GPS receiver phase-locked tracking loops and eventually cause the receivers to lose lock. Loss of lock in this profile occurred at approximately 11:50 UTC when the signal was 3.9° below the horizon for PRN25 (corresponding to a tangent height of approximately 4 km above the surface). Loss of lock by the GISMOS geodetic receivers occurred above 5 km for all other occultations from this flight (Figure 2) and the other flights into the pre-Karl system. For that reason, GISMOS was designed

with a raw RF sampling GPS recording system (GRS) where open loop tracking could mitigate this effect. Open loop tracking was developed to replace the traditional feedback loop with a method that tracks the signal using an a priori estimate of Doppler shift, as described in *Beyerle et al*. [2006], rather than determining the Doppler shift from the signal itself. The method has been implemented in a software receiver and adapted to the signal dynamics of the airborne system [*Lulich et al*., 2010; *Wang et al*., 2013]. We applied this open loop tracking to the raw 10 MHz RF data recorded by the GRS in postprocessing mode. The result for the same PRN25 occultation is shown in Figure 3c (dashed line) and extends the profile an additional 2 km further toward the surface. The open loop RO profile also shows similar agreement with the coincident dropsonde measurement. The high-moisture environment of the subtropics is a challenging environment for the conventional GPS receivers, and a preliminary inventory of the remainder of the data set shows that recordings down to ~ 6 km occurred for less than one profile per flight or a total of 21 profiles for 26 flights during the entire PREDICT campaign. In comparison, the preliminary analysis of the GRS data from one flight using the open loop method indicates that excess phase was recovered down to a height corresponding to 2 km for both rising and setting satellites for more than seven occultations per flight. The further analysis of the complete GISMOS GRS data set in the future will therefore provide an optimal data set for both a robust statistical study as well as an exceptional data set for assimilation. This proof of concept presents the potential for developing an operational system based on an upgraded GPS receiver that could be deployed on commercial aircraft, which are already equipped with inertial navigation systems and external GPS antennas. We have compared open loop tracking signals from the top and side-looking antennas (not shown) and find that refractivity results differ by less than 0.5%. This illustrates that the inertial navigation system navigation solution is accurate enough when transferred to the location of the side or top antenna [see also *Muradyan et al*., 2010]. Although the GRS data from the top antenna terminated at 4 km altitude rather than 2 km for the side antenna, it illustrates that data from a simpler installation using the top antenna for occultations on commercial aircraft would still be worthwhile.

4. Conclusions

The GNSS Instrument System for Multistatic and Occultation Sensing (GISMOS) has been developed for airborne high-vertical resolution atmospheric profiling of regional meteorological targets such as developing tropical storms, where assimilation of observations in the upstream environment has the potential to improve forecast accuracy. In August and September 2010, GISMOS was deployed on the National Science Foundation Gulfstream-V aircraft to make atmospheric observations in the southeastern Atlantic and Caribbean during the Pre-Depression Investigation of Cloud systems in the Tropics (PREDICT), with concurrent sampling by dropsondes. Despite the relatively large-horizontal averaging length of the limb-sounding occultations, the retrieved refractivity values at the tangent points agreed to better than 2% with the measurements from the closest dropsonde. This is sufficient to distinguish the order of magnitude variations in refractivity observed by dropsondes between developing and nondeveloping cases quantified by other researchers during the PREDICT campaign, and the temporal changes in refractivity associated with moisture changes in the last 72 h prior to genesis in the 150 km region around the circulation center, as demonstrated by *Komaromi* [2013]. GISMOS has the capability for 10 MHz sampling of the RF data, which when combined with a software receiver that performs open loop tracking, significantly extends its measurement capability in the lower troposphere as low as 2 km, for both rising and setting satellites. The repeatability of the measurements, shown by the agreement between the independent measurements made by conventional geodetic measurement system and the GRS, is better than 0.5% refractivity. The open loop method has the ability to recover on the order of 1–2 profiles for each hour of flight time, and thus would be a valuable method to develop for real-time operational use. The method is less accurate than spaceborne radio occultation, as a consequence of the turbulent aircraft motion. However, the aircraft deployments can provide many more profiles in the storm region or a region of interest than are possible with the current combination of spaceborne GPS RO missions, and thus, they provide a unique data set for testing the impact of assimilating a dense suite of occultation measurements. In combination with the dropsondes, airborne RO increases by 50% the number of profiles that will be available for studying the development of storm systems within tropical waves during the PREDICT campaign. The technique has the potential to provide hundreds of profiles per day if implemented on commercial aircraft for use in operational data assimilation in numerical weather models. Airborne RO could thus be an important addition to the atmospheric observation system for tropical storms.

Acknowledgments

Support for this work was provided by HIAPER UCAR subcontract S05-39696 from NSF, NSF grant SGER-0802887, and NSF grant AGS 1015904. Partial support for B.M. was provided by the Ross Fellowship. P.M. was supported by the Schlumberger Faculty for the Future Fellowship. F.G.N. was supported by a Capes/Fulbright Graduate Student Fellowship (1834/07-0) and a NASA Earth System Science Research Fellowship (NNX11AL50H). We would also like to thank the following: A. Johnson who assisted with the GISMOS data collection; J. Jensen, J. Meitin, A. Cooper, A. Schanot, R. Sherman, and the NCAR-EOL staff for logistical support; PREDICT principal investigato M. Montgomery and C. Davis; M. Bell, D. Raymond, and C. Lopez who assisted with GISMOS operation; J. Dunion, J. Cordeira, K. Griffin, and the PREDICT/NASA/NOAA forecast teams; and K. Young, J. Wang, and the NCAR-EOL dropsonde team. We would like to acknowledge the continued support and interest of NSF program officers, in particular J. Fein and E. DeWeaver, B. Smull, and J. Huning. We acknowledge the infrastructure and expertise provided by E. Calais at the Geodesy Laboratory at Purdue (now at Ecole Normale Superieur, Paris) during the early development of the airborne RO system.

The Editor thanks two anonymous reviewers for their assistance in evaluating this paper.

References

Anthes, R. A., et al. (2008), The COSMIC/FORMOSAT-3 Mission: Early results, *Bull. Am. Meteorol. Soc.*, *89*(3), 313–333.

Beyerle, G., T. Schmidt, J. Wickert, S. Heise, M. Rothacher, G. Konig-Langlo, and K. B. Lauritsen (2006), Observations and simulations of receiver-induced refractivity biases in GPS radio occultation, *J. Geophys. Res.*, *111*, D12101, doi:10.1029/2005JD006673.

Chen, S.-Y., C.-Y. Huang, Y.-H. Kuo, Y.-R. Guo, and S. Sokolovskiy (2009), Assimilation of GPS refractivity from FORMOSAT-3/COSMIC using a nonlocal operator with WR 3DVAR and its impact on the prediction of a typhoon event, *Terr. Atmos. Oceanic Sci.*, *20*, 133–154.

Chen, S.-Y., C.-Y. Huang, Y.-H. Kuo, and S. Sokolovskiy (2011), Observational error estimation of FORMOSAT-3/COSMIC GPS radio occultation data, *Mon. Weather Rev.*, *139*, 853–865.

Dunkerton, T. J., M. T. Montgomery, and Z. Wang (2008), Tropical cyclogenesis in a tropical wave critical layer: Easterly waves, *Atmos. Chem. Phys. Discuss.*, *8*, 11,149–11,292.

Frehlich, R. (2011), The definition of "truth" for numerical weather prediction error statistics, *Q. J. R. Meteorol. Soc.*, *137*(654), 84–98.

Garrison, J. L., M. Walker, J. S. Haase, T. Lulich, F. Xie, B. D. Ventre, M. H. Boehme, B. Wilmhoff, and S. J. Katzberg (2007), Development and testing of the GISMOS instrument, paper presented at IEEE International Geoscience and Remote Sensing Symposium, Barcelona, Spain, 23-27 July 2007, 1-4.

Healy, S. B., and J. N. Thepaut (2006), Assimilation experiments with CHAMP GPS radio occultation measurements, *Q. J. R. Meteorol. Soc.*, *132*(615), 605–623.

Healy, S. B., J. Haase, and O. Lesne (2002), Abel transform inversion of radio occultation measurements made with a receiver inside the Earth's atmosphere, *Ann. Geophys.*, *20*(8), 1253–1256.

Huang, C. Y., Y.-H. Kuo, S.-H. Chen, and F. Vandenberghe (2005), Improvements on typhoon forecasting with assimilated GPS occultation refractivity, *Weather Forecast.*, *20*(6), 931–953.

Huang, C.-Y., et al. (2010), Impact of GPS radio occultation data assimilation on regional weather predictions, *GPS Solutions*, *14*(1), 35–49.

Komaromi, W. A. (2013), An investigation of composite dropsonde profiles for developing and nondeveloping tropical waves during the 2010 PREDICT field campaign, *J. Atmos. Sci.*, *70*(2), 542–558.

Kueh, M.-T., C.-Y. Huang, S.-Y. Chen, S.-H. Chen, and C.-J. Wang (2009), Impact of GPS radio occultation refractivity soundings on a simulation of Typhoon Bilis (2006) upon landfall, *Terr. Atmos. Oceanic Sci.*, *20*(1), 115–131.

Kursinski, E. R., et al. (1996), Initial results of radio occultation observations of Earth's atmosphere using the global positioning system, *Science*, *271*(5252), 1107–1110.

Landsea, C. W. (1993), A climatology of intense (or major) Atlantic hurricanes, *Mon. Weather Rev.*, *121*, 1703–1713.

Lesne, O., J. Haase, G. Kirchengast, J. Ramsauer, and W. Poetzi (2002), Sensitivity analysis for airborne sounding of the troposphere by GNSS radio occultation, *Phys. Chem. Earth*, *27*(4-5), 291–299.

Liu, H., J. Anderson, and Y.-H. Kuo (2012), Improved analyses and forecasts of Hurricane Ernesto's genesis using radio occultation data in an ensemble filter assimilation system, *Mon. Weather Rev.*, *140*(1), 151–166.

Lulich, T. D., J. L. Garrison, J. S. Haase, Y.-M. Yang, J. Voo, F. Xie, and P. Muradyan (2010), Open loop tracking of radio occultation signals from an airborne platform, paper presented at the 23rd International Technical Meeting of the Satellite Division of the Institute of Navigation (ION GNSS 2010), Portland, Oregon, September 21-24, 2010., 1049-1060.

Montgomery, M. T., et al. (2012), The Pre-Depression Investigation of Cloud Systems in the Tropics (PREDICT) experiment: Scientific basis, new analysis tools and some first results, *Bull. Am. Meteorol. Soc.*, *92*(9), 153–172.

Muradyan, P. (2012), Profiling the atmosphere with the airborne GPS radio occultation technique using open-loop tracking, PhD thesis, 196 pp, Purdue University, West Lafayette, IN, U.S.A.

Muradyan, P., J. S. Haase, F. Xie, J. L. Garrison, T. Lulich, and J. Voo (2010), GPS/INS navigation precision and its effect on airborne radio occultation retrieval accuracy, *GPS Solutions*, doi:10.1007/s10291-010-0183-7.

Parrish, D. F., and J. C. Derber (1992), The National Meteorological Centers spectral statistical interpolation analysis system, *Mon. Weather Rev.*, *120*(8), 1747–1763.

Poli, P., S. B. Healy, F. Rabier, and J. Pailleux (2008), Preliminary assessment of the scalability of GPS radio occultations impact in numerical weather prediction, *Geophys. Res. Lett.*, *35*, L23811, doi:10.1029/2008GL035873.

Rüeger, J. (2002), Refractive index formulae for electronic distance measurements with radio and millimetre waves, Rep. Unisurv Rep. 109, 758-766 pp, University of New South Wales, Sydney, Australia.

Stewart, S. R. (2011), Tropical cyclone report, Hurricane Karl, Rep., 17 pp, National Hurricane Center, Miami, FL.

Wang, K.-N., P. Muradyan, J. L. Garrison, J. S. Haase, B. Murphy, U. Acikoz, and T. Lulich (2013), Open-loop tracking of rising and setting GNSS radio-occultation signals from an airborne platform: Signal model and statistical analysis, paper presented at IEEE International Geoscience and Remote Sensing Symposium, Melbourne, Australia, 21-26 July 2013.

Wang, Z., M. T. Montgomery, and T. J. Dunkerton (2010), Genesis of Pre-Hurricane Felix (2007). Part I: The Role of the easterly wave critical layer, *J. Atmos. Sci.*, *67*(6), 1711–1729.

Weissmann, M., and C. Cardinali (2007), Impact of airborne Doppler lidar observations on ECMWF forecasts, *Q. J. R. Meteorol. Soc.*, *133*(622), 107–116.

Xie, F., J. S. Haase, and S. Syndergaard (2008), Profiling the atmosphere using the airborne GPS radio occultation technique: A sensitivity study, *Trans. IEEE Geosci. Remote Sens.*, *46*(11), 3424–3435.

Yoshihara, T., N. Fujii, S. Saitoh, T. Sakai, K. Matsunaga, K. Hoshinoo, T. Tsuda, Y. Aoyama, and S. Danno (2006), Airborne-based downward-looking GPS occultation experiments, *IEICE Trans.*, *J89-B*(7), 1233–1241.

Zuffada, C., G. Hajj, and E. R. Kursinski (1999), A novel approach to atmospheric profiling with a mountain-based or airborne GPS receiver, *J. Geophys. Res.*, *104*(D20), 24,435–24,447.

Supplementary Information:

First Results from an Airborne GPS Radio Occultation System for Atmospheric Profiling

J. S. Haase[1], B.J. Murphy[2], P. Muradyan[2], F.G. Nievinski[3], K.M. Larson[4], J. L. Garrison[5], K.-N. Wang[5]

[1]*Scripps Institution of Oceanography, University of California San Diego, La Jolla, CA 92093-0225*

[2]*Dept. of Earth, Atmospheric, and Planetary Sciences, Purdue University, West Lafayette, IN 47907-2051*

[3] *Faculdade de Ciências e Tecnologia, Universidade Estadual Paulista, Presidente Prudente, SP, Brazil*

[4]*Dept of Aerospace Engineering Sciences, University of Colorado, Boulder, CO 80309-0429*

[5]*Dept. of Aeronautics & Astronautics Engineering, Purdue University, West Lafayette, IN 47907*

Corresponding Author:

Jennifer S. Haase

858-534-8771

858-534-9833 (fax)

jhaase@ucsd.edu

1. Method

The method for retrieving atmospheric properties from spaceborne radio occultation measurements has been described in the literature [*Hajj et al.*, 2002; *Kursinski et al.*, 1997]. Modifications to this basic approach have been derived for the airborne geometry [*Healy et al.*, 2002; *Lesne et al.*, 2002; *Xie et al.*, 2008], which we have implemented here. We assume the formula for refractive index of the neutral atmosphere at GPS frequencies neglecting incompressibility [*Healy*, 2011; *Rüeger*, 2002] is

$$N = (n-1)\times 10^6 = \frac{77.6890\ P}{T} - \frac{6.3938e}{T} + \frac{3.75463\times 10^5 e}{T^2} \quad (1)$$

where N is refractivity, n is the refractive index, P is the atmospheric pressure [hPa], T is atmospheric temperature [K], and e is water vapor partial pressure [hPa]. Assuming a spherical atmosphere [*Born and Wolf*, 1964], the integrated bending angle, α_N, caused by refraction for a negative elevation angle ray is modified for the airborne case to include two terms (Healy et al., 2002; Lesne et al., 2002)

$$\alpha_N(a) = -2a\int_{r_t}^{r_R} \frac{1}{\sqrt{n^2r^2-a^2}} \frac{d(\ln n)}{dr} dr - a\int_{r_R}^{r_T} \frac{1}{\sqrt{n^2r^2-a^2}} \frac{d(\ln n)}{dr} dr \quad (2)$$

where r_R is the distance from the center of curvature of the Earth to the GPS receiver, r_T is the distance to the GPS transmitter, and r_t is the distance to the tangent point. The impact parameter a is given by Bouger's law

$$a = n_t \cdot r_t = n_T \cdot r_T \cdot \sin\phi_T = n_R \cdot r_R \cdot \sin\phi_R = n(r) \cdot r \cdot \sin\phi \ = \ constant \quad (3)$$

along a given ray. Here, ϕ_R is the angle between the radius vector r_R and the ray path for the ray reaching the receiver from below the horizon. There is a positive elevation angle ray reaching the receiver from above the horizon with the same impact parameter:

$$n_R \cdot r_R \cdot \sin\phi_R = n_R \cdot r_R \cdot \sin(\pi - \phi_R) \quad (4)$$

40 The right hand term of equation 2 is equivalent to the bending accumulated for the positive elevation
41 angle ray, α_P. Subtracting a value for the positive elevation angle ray, either observed or simulated,
42 leaves a symmetric integral of refractive index for the partial bending angle defined as

43 $$\alpha'(a) = \alpha_N(a) - \alpha_P(a) = -2a\int_{r_t}^{r_R} \frac{1}{\sqrt{n^2r^2 - a^2}} \frac{d(\ln n)}{dr} dr \quad (5)$$

44 which can be solved for refractive index as a function of distance from the center of curvature r using
45 the Abel transform

46 $$n(r) = n_R \exp\left(\frac{1}{\pi} \int_{a_r}^{a_R} \frac{\alpha'(a)}{\sqrt{a^2 - a_r^2}} da \right). \quad (6)$$

47 Therefore, the bending angle must be derived from the GPS observations in order to retrieve the
48 refractive index profile. The refractive bending of the ray path induces an excess Doppler shift in the
49 carrier phase of the GPS signal, which is the fundamental observed quantity. The projection of the
50 satellite orbital motion in the direction of the refracted signal ray path produces a Doppler shift, f_d, in the
51 GPS transmitter frequency, f_T.. After correction for relativistic effects the Doppler shift is given by
52 [*Kursinski et al.*, 1997; *Vorobe'ev and Krasil'nikova*, 1994]

53 $$f_d = -\frac{f_T}{c}\left(n_T V_T^r cos\phi_T + n_T V_T^\theta \sin\phi_T + n_R V_R^r cos\phi_R - n_R V_R^\theta \sin\phi_R\right) \quad (7)$$

54 where V^r and V^θ are the radial and azimuthal components of velocity, respectively, for the receiver,
55 indicated by the subscript R, and transmitter, T. The bending is calculated iteratively from the observed
56 Doppler shift (equation 7), Bouguer's law (equation 3), and the additional geometrical constraint

57 $$\phi_T + \phi_R + \theta - \pi = \alpha \quad (8).$$

58 The dependence on both e and T in equation 1 leads to an ambiguity in the retrieval of humidity
59 profiles from the refractivity. The water vapor profile can be retrieved if an *a priori* temperature profile
60 from climatology or a numerical weather model, is available, and hydrostatic equilibrium is assumed.

Alternatively, bending angle or refractivity observations can be directly validated or assimilated into numerical models. Our approach is to directly compare the refractivity with refractivity derived from dropsonde profiles, in order to address the accuracy of the measurement to be assimilated with as few assumptions as possible.

To implement this approach for the airborne dataset, the geometric range from the antenna to the satellite was calculated and then subtracted from the observed carrier phase to produce the excess phase. The excess phase was also corrected for relativistic effects, ionospheric delay using the dual-frequency measurements, and satellite clock error provided along with the precise ephemerides from the IGS. The excess phase (in meters) was time differentiated to produce the phase-rate or excess Doppler (in m/s), which also cancels out carrier phase ambiguities. The excess Doppler was calculated for the occulting satellite as well as one simultaneously recorded high elevation satellite. The excess Doppler from the high elevation satellite was subtracted from that of the occulting satellite to remove the receiver clock error. The excess Doppler difference was then filtered using a 4^{th} order Savitzky Galoy filter with a 2 second span.

We solved for the bending angle using the approach described by equations 3, 7, and 8 above [*Vorobe'ev and Krasil'nikova*, 1994]. This required an estimate of the refractive index at the transmitter height, which can be safely taken as $n_T = 1$, and at the aircraft height. We used the flight-level temperature and pressure recorded by the in-situ sensors in equation 1 to estimate n_R, neglecting the water vapor contributions. Moisture was not measured by in-situ sensors during the campaign, however the effects of the low moisture present at 14 km flight altitude were assumed to be negligible, relative the expected refractivity errors given at that height in simulation studies (Muradyan, 2010). The retrieved bending angle is shown in Figure 3b. Noise in the Doppler shift due to aircraft turbulence and

navigation error creates large errors in bending angle near the maximum impact parameter, yet the value of a_{max} converges to a precise value.

We carried out the refractivity retrieval in three steps. First, the partial bending angle was calculated for each value of impact parameter, given the noisy observed bending angle profile (Figure 3b; gray line). Then the partial bending angle was inverted using the Abel transform in equation 6 to retrieve an initial estimate of the refractivity profile, which was poorly determined near the height of the aircraft. The refractivity profile was then fit using a series of Fourier coefficients to the aircraft height, then extrapolated above the aircraft height using an exponential function with a 7 km scale height to produce a smooth refractivity profile that is continuous at the aircraft height and consistent with the in-situ refractivity. In the second step, the smooth Fourier fit profile was used to calculate bending angle using equation 2. The noisy observed bending angle observations were replaced with the smooth simulated bending angle values for all values of impact parameter above 1 km below the aircraft height (Figure 3**Error! Reference source not found.**b; black line). The partial bending angle was calculated from this merged bending angle profile. In the third step, this smooth partial bending angle profile was inverted for the final refractivity profile, once again using the Abel transform in equation 6.

2. Measurement System

The GISMOS system makes continuous observations of GPS code pseudorange and carrier phase on the L1 (1.57542 GHz) and L2 (1.22760 GHz) frequencies from custom high-gain side-looking antennas and commercial lower gain avionics antennas, also side-looking. Each of these antennas provides input to a dual-frequency Trimble NetRS GPS receiver sampling at 5 Hz. In addition, the RF signal from each of the high-gain antennas is also routed to a GNSS Recording System (GRS), which is capable of continuously sampling both L1 and L2 frequencies at 10 MHz for post-processing using an open-loop software receiver. A Sensor Systems avionics L1/L2 GPS antenna mounted on the top of the aircraft

fuselage feeds an Applanix POS/AV inertial navigation system, which samples GPS at 10 Hz and is aided by a high-grade Inertial Science inertial measurement unit (IMU) at 200 Hz [*Garrison et al.*, 2007]. The precise position and velocity of the aircraft were calculated using the Applanix POSPac MMS post-processing software [*Mostafa and Hutton*, 2001] using a tightly coupled Kalman filter GPS-IMU solution. Precise final orbits and clocks were used from the International GNSS Service [*Beutler et al.*, 2009; *Beutler et al.*, 1999]. The position precision is better than 6 cm in the horizontal and 90 cm in the vertical, and velocity precision is better than 5 mm/s in all components [*Muradyan et al.*, 2010] as required for accurate airborne retrievals [*Muradyan*, 2012; *Xie et al.*, 2008]. Flight level in-situ temperature and pressure were measured at 50 Hz with a fast response de-iced Rosemount Model 102AL TAT sensor with ±0.5 C accuracy and a Paroscientific Model 1000 Digiquartz transducer with and ±1 hPa accuracy, respectively.

3. References

Beutler, G., A. Moore, and I. Mueller (2009), The international global navigation satellite systems service (IGS): development and achievements, *Journal of Geodesy*, *83*(3-4), 297-307.

Beutler, G., M. Rothacher, S. Schaer, T. A. Springer, J. Kouba, and R. E. Neilan (1999), The International GPS Service (IGS): An interdisciplinary service in support of Earth sciences, *Advances in Space Research*, *23*(4), 631-653.

Born, M., and E. Wolf (1964), *Principles of Optics: Electromagnetic Theory of Propagation, Interference and Diffraction of Light*, 856 pp., Pergamon Press.

Garrison, J. L., M. Walker, J. S. Haase, T. Lulich, F. Xie, B. D. Ventre, M. H. Boehme, B. Wilmhoff, and S. J. Katzberg (2007), Development and Testing of the GISMOS Instrument, *Proceedings of the IEEE International Geoscience and Remote Sensing Symposium*, 1-4.

129 Hajj, G. A., E. R. Kursinski, L. J. Romans, W. I. Bertiger, and S. S. Leroy (2002), A technical
130 description of atmospheric sounding by GPS occultation, *Journal of Atmospheric and Solar-Terrestrial*
131 *Physics*, *64*(4), 451-469.
132 Healy, S. B. (2011), Refractivity coefficients used in the assimilation of GPS radio occultation
133 measurements, *Journal of Geophysical Research*, *116*(D1), D01106.
134 Healy, S. B., J. Haase, and O. Lesne (2002), Abel transform inversion of radio occultation
135 measurements made with a receiver inside the Earth's atmosphere, *Annales Geophysicae*, *20*(8), 1253-
136 1256.
137 Kursinski, E. R., G. A. Hajj, K. R. Hardy, J. T. Schofield, and R. Linfield (1997), Observing Earth's
138 atmosphere with radio occultation measurements, *J. Geoph. Res.*, *102*(23), 23.429-423.465.
139 Lesne, O., J. Haase, G. Kirchengast, J. Ramsauer, and W. Poetzi (2002), Sensitivity analysis for airborne
140 sounding of the troposphere by GNSS radio occultation, *Phys. and Chem. of the Earth*, *27*(4-5), 291-
141 299.
142 Mostafa, M. M. R., and J. Hutton (2001), Direct positioning and orientation systems. How do they
143 work? What is the attainable accuracy?, paper presented at American Society of Photogrammetry and
144 Remote Sensing Annual Meeting, St. Louis, MO, USA, April 24-27, 2001.
145 Muradyan, P. (2012), Profiling the atmosphere with the airborne GPS radio occultation technique using
146 open-loop tracking, PhD thesis, 196 pp, Purdue University, West Lafayette, IN, USA.
147 Muradyan, P., J. S. Haase, F. Xie, J. L. Garrison, T. Lulich, and J. Voo (2010), GPS/INS navigation
148 precision and its effect on airborne radio occultation retrieval accuracy, *GPS Solutions*, *10.1007/s10291-*
149 *010-0183-7*.

Rüeger, J. (2002), Refractive index formulae for electronic distance measurements with radio and millimetre waves*Rep. Unisurv Rep. 109*, 758-766 pp, University of New South Wales, Sydney, Australia.

Vorobe'ev, V. V., and T. G. Krasil'nikova (1994), Estimation of the accuracy of the atmospheric refractive index recovery from Doppler shift measurements at frequencies used in the NAVSTAR system, *Physics of the Atmosphere and Ocean (English Translation)*, *29*(5), 602-609.

Xie, F., J. S. Haase, and S. Syndergaard (2008), Profiling the Atmosphere Using the Airborne GPS Radio Occultation Technique: A Sensitivity Study, *Trans. IEEE Geosci. and Remote Sens.*, *46*(11), 3424-3435.